Semnan University

Journal of Modeling & Simulation in Electrical & Electronics Engineering (MSEEE)

Journal homepage: **https://mseee.semnan.ac.ir/**

ISSN: 2821-0786

Design and Optimization of a Rose-Inspired Plasmonic Filter using Machine Learning

Seyed Mohammad Mehdi Hosseini[1], Pejman Rezaei[2]*and Shiva Khani[3]

***Abstract*- Bio-inspired plasmonic structures offer a powerful route toward compact and high-performance photonic components by ena-bling strong confinement of surface plasmon polaritons (SPPs) at deeply subwavelength scales. In this research, a tunable mul-tichannel bandpass filter using surface plasmon polaritons (SPPs) is introduced and numerically studied on a metal-insulator-metal (MIM) waveguide substrate. Consisting of a central circular resonator, two larger main waveguides, and six smaller sat-ellite resonators, the proposed structure exploits a unique rose-like geometry. High Q-factor (Q-factor) multiple resonance modes can be achieved due to this blend. Nevertheless, time-consuming numerical methods such as the Finite-Difference Time-Domain (FDTD) approach are employed in the conventional design and optimization of such intricate structures. Re-cently, a machine learning framework was utilized to considerably accelerate the design procedure. Through training on a vast dataset from FDTD runs, a Random Forest surrogate model was developed and trained to predict the filter spectral response from its geometrical parameters with very high accuracy. FDTD simulation results reveal that the proposed rose-like structure produces several sharp transmission peaks of high Q-factor, up to 127.2. Moreover, the machine learning system possesses a high coefficient of determination (R^2 up to 0.986) and excellent predictive ability and can replicate the transmission spectrum within a fraction of the time it takes for conventional runs. Through its powerful volume-based optimization tool and inverse design tool, the proposed mixed-method approach brings within grasp possible future applications of photonic integrated circuits (PICs), high-sensitivity biosensors, and wavelength-division multiplexing (WDM) systems.**

***Index Terms*: Plasmonic Filter, MIM Waveguide (Metal-Insulator-Metal), Circular Resonator, Machine Learning, Quality Fac-tor.Introduction**

I. INTRODUCTION

The rapid growth of modern information technology [1] has contributed to a considerable demand for increased integration density of photonic devices over the past several years. The use of surface plasmon polaritons (SPPs), which are transverse electromagnetic waves propagating at the interface of a metal and a dielectric, represents a promising direction in developing ultra-high-density photonic integrated circuits (PICs) [2, 3]. Structures based on SPPs allow for manipulating light at the sub-wavelength scale, thereby overcoming the traditional diffraction limit of dielectric waveguides [4-6]. Among numerous SPP platforms for building highly integrated optical circuits, metal-insulator-metal (MIM) waveguides are one of the most com-mon. Such waveguides provide many advantages, including strong subwavelength light confinement, decreased propagation losses, and simple fabrication procedures [6, 7]. Various optical devices utilizing SPP structures have been proposed by re-searchers, such as plasmonic filters, demultiplexers, splitters, and sensors [8-28]. Plasmonic filters play an essential role in frequency selection within systems such as wavelength-division multiplexing (WDM) and refractive index sensing [10]. The main targets for these devices are to have a high-quality factor (Q-factor), high transmission efficiency, and an optimal figure of merit (FOM) for enabling their integration in photonics [11, 12]. In recent years, bio-inspired structures that mimic those found in nature, such as butterfly wings or diatom shells, have emerged as novel approaches to create distinctive optical

Received; 2025-10-10 Revised; 2025-12-20 Accepted; 2025-12-28

1. Electrical and Computer Engineering Faculty, Semnan University, Semnan, Iran.
2. Electrical and Computer Engineering Faculty, Semnan University, Semnan, Iran.
3. Electrical and Computer Engineering Faculty, Semnan University, Semnan, Iran.
*Corresponding author: prezaei@semnan.ac.ir

Cite this article as:
Hosseini, S. M. M., Rezaei, P., & Khani, S. (2025). Design and Optimization of a Rose-Inspired Plasmonic Filter using Machine Learning. *Journal of Modeling & Simulation in Electrical & Electronics Engineering (MSEEE)*. Semnan University Press. 6 (1), 43-51.
DOI: https://doi.org/10.22075/MSEEE.2025.39313.1231

prop-erties as well as increase the interaction of light with matter [13-15, 19, 20]. However, the analysis, along with optimization of these nanophotonic structures, traditionally makes use of electromagnetic simulation software based on time-consuming methods, such as the Finite-Difference Time-Domain (FDTD) technique [2]. The numerical approach used requires exhaustive trial-and-error searches over the geometric parameters of the device, an exercise that is computationally intensive and ineffi-cient. In response to such a design challenge, machine learning (ML) algorithms have emerged as an effective solution for building surrogate models capable of rapid and accurate prediction of the spectral properties of a device [1, 16, 29-33]. This AI-assisted approach provides an efficient and reliable means for the inverse design and rapid optimization of complex nano-photonic devices [17, 18]; an approach that has been explored by researchers such as Khani et al for the analysis of plasmonic sensors [1]. In this paper, we combine a novel and high-performance design for a plasmonic filter with an efficient machine learning framework. We propose a multichannel bandpass filter with a unique, rose-inspired geometry on a MIM waveguide platform. First, the performance of this structure is analyzed using the FDTD method to determine its tunable and multichan-nel response. Then, we demonstrate that a Random Forest Regressor, trained on FDTD simulation data, can serve as a powerful surrogate model for accurately predicting the filter's spectral characteristics.

II. METHOD FOR DESIGNING AND SIMULATING STRUCTURES

The proposed plasmonic filter, as shown in Fig. 1, is based on a MIM structure in which air acts as the insulator. The device is arranged on a plasma substrate, and air serves as the dielectric around it. The structure has two main waveguides and a com-plicated system of resonators. The resonator is based on the shape of a rose. It has a central circular cavity with a radius of 300 nm and six smaller satellite circular cavities with a radius of 150 nm.

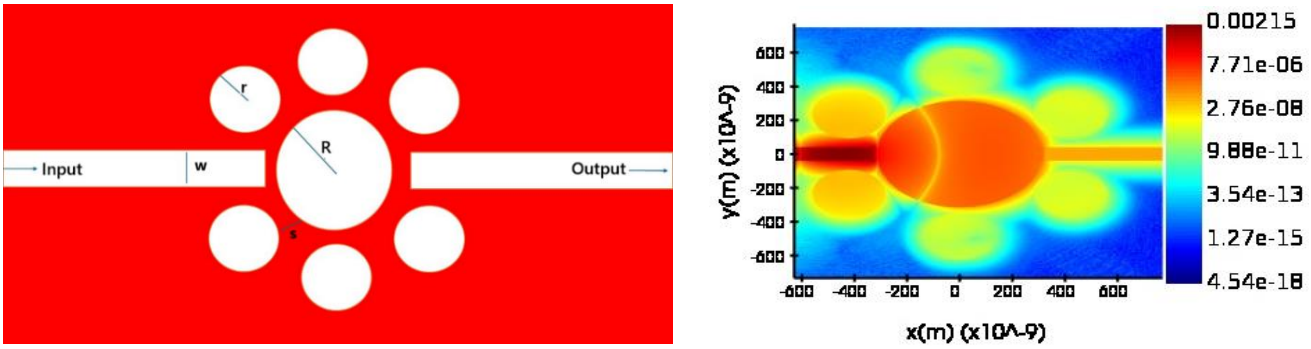

(a) (b)

Fig. 1. (a) Schematic of the proposed rose-inspired plasmonic filter, specifying the key geometric parameters: main resona-tor radius (R), small resonator radius (r), waveguide width (w), and the gap between the central and satellite resonators (s). (b). Electric field distribution in the rose-inspired plasmonic filter at one of the resonance modes. Warmer colors (red and orange) indicate higher field intensity, and cooler colors (blue) indicate lower field intensity. This distribution indicates the effective coupling between the central and satellite resonators.

The main waveguides are also 50 nm wide. Additionally, the electric field distribution in the proposed structure is depicted in Fig. 1 (inset). This image clearly illustrates the interaction and coupling of light within the resonators and the waveguide.

$$\varepsilon(\omega)=\varepsilon_{\infty}-(\omega_p^2)/(\omega^2-i\gamma\omega) \quad (1)$$

The frequency-dependent complex relative permittivity of silver for all components, including the substrate, is characterized by the Drude model:

The parameters for this model were obtained by fitting the experimental data of Palik in the Lumerical software environment, and the following values were used for all simulations: permittivity at infinite frequency $\varepsilon_{\infty}=3.4611$, bulk plasma frequency $\omega_p=9.0264$ eV, and electron collision frequency $\gamma=0.051111$ eV.

All numerical simulations were performed using the commercial FDTD software package from Lumerical. To reduce computational costs, a two-dimensional (2D-FDTD) simulation model was used. The simulation domain was set to 3 μm × 3 μm, and at all boundaries, perfectly matched layer (PML) boundary conditions were used to absorb outgoing waves. To ensure high accuracy, a fine mesh grid with a uniform step of $\Delta x=\Delta y=3$ nm was used. A Mode Source was used to excite the fundamental TM plasmonic mode in the input waveguide, and a frequency-domain field and power monitor was placed at the output to calculate the transmission spectrum ($T=P_{output}/P_{input}$) in the wavelength range of 400 to 1800 nm.

III. MACHINE LEARNING MODEL

To build an effective surrogate of time-costly FDTD computations, a supervised machine learning approach was used. Machine learning offers a quicker substitute to explicit electromagnetic modeling by acquiring the nonlinear transformation from geometrical parameters to optical response non-iteratively, rather than solving Maxwell's equations. A Random Forest Regressor was chosen, as this ensemble learning technique has strong resilience to overfitting and has robust performance even with smaller training sets.

A narrow, high-performance range was systematically swept on three important geometric parameters and used to generate a concentrated dataset of 90 individual FDTD runs. Although this dataset is short, it is carefully chosen

to be optimally appropriate for our task: developing a highly precise local surrogate model used for fine-tuning a previously promising design, rather than laboriously sampling the complete global parameter space. This selective approach permits a powerful yet computationally efficient optimization procedure. The main resonator radius (R) was swept between 290 nm and 310 nm, the satellite resonator radius (r) between 140 nm and 160 nm, and the gap (s) was tuned within values between -10 nm and +10 nm. For each simulation, the model's inputs were the three geometrical parameters [R, r, s], and the output was the corresponding transmission spectrum at 1401 discrete points within a wavelength interval of 400-1800 nm. Only then was the dataset normalized, shuffled, and divided into training and test sets in order to produce unbiased performance measures. The learned model sufficiently recreated FDTD-simulated spectra with a very high coefficient of determination (R^2>0.95) significantly lowered the design cycle and made real-time optimization feasible.

IV. RESULTS AND DISCUSSION

In this section, the step-by-step design and optimization process of the proposed plasmonic filter, from a basic structure to the final geometry, is presented and analyzed.

A. Initial Design and Bio-Inspiration

Our design process began with a basic and conventional structure in plasmonic filters: namely, a single circular resonator coupled to two MIM waveguides (Fig. 2a). Although this simple structure is capable of generating resonance modes, it usually has limitations in terms of the number of channels and the quality factor (Q-factor). To improve the performance and achieve a more complex and efficient spectral response, we drew inspiration from nature. Inspired by the symmetry and structure of a rose, six smaller circular resonators (satellites) were added around the central resonator (Fig. 2b). This hexagonal symmetry, analogous to photonic crystal structures, facilitates complex mode coupling between the resonators, which is essential for enhancing the quality factor and creating multiple channels.

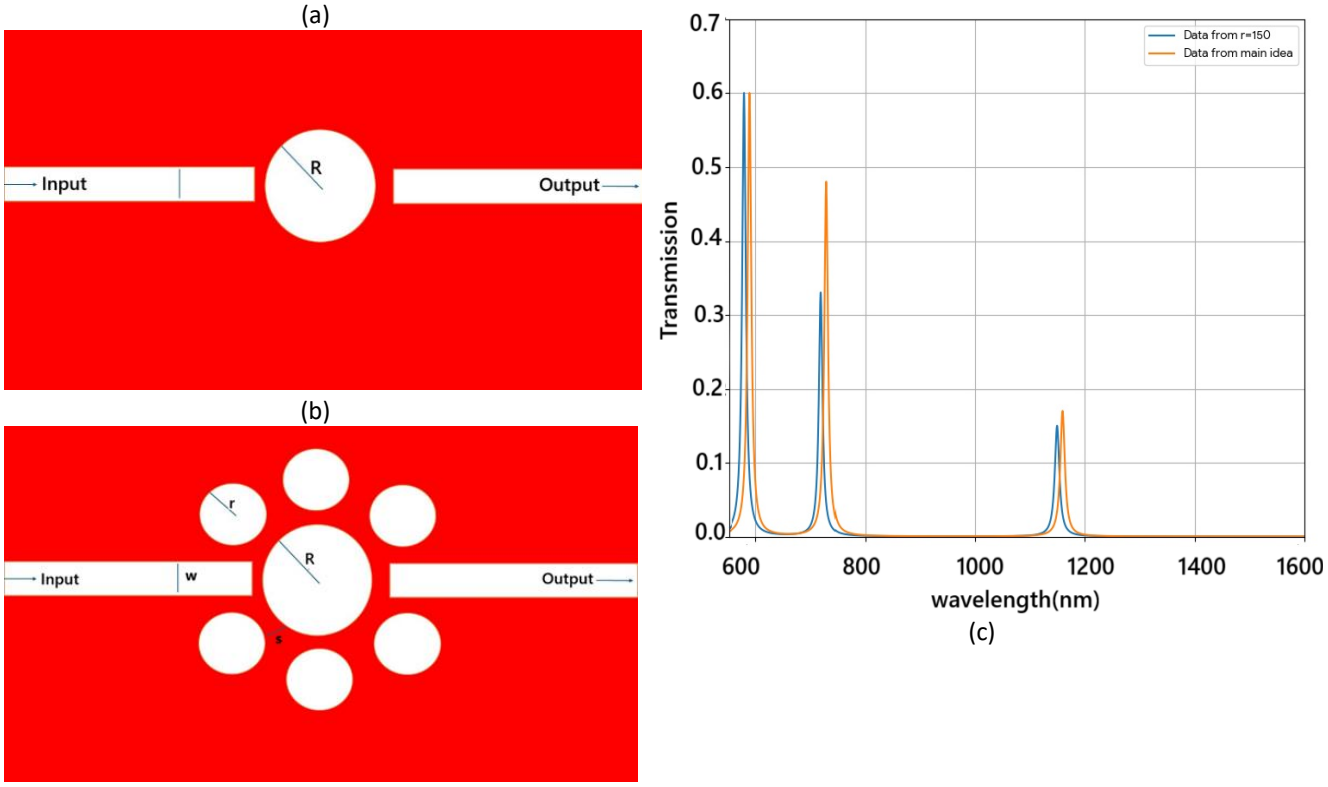

Fig. 2. (a) Schematic of the initial structure with a single circular resonator. (b) The final rose-inspired structure, with the addition of six satellite resonators. (c) Comparison of the transmission spectra, showing that the final rose-inspired structure (Data from r=150) generates additional, sharper transmission peaks compared to the initial structure.

The center-to-center distance between the main resonator and each small resonator was determined by considering a fixed gap of 20 nm. The objective of this design was to create a more complex coupling between different modes, thereby generating multiple resonance peaks with higher quality. As shown in Fig. 2c and 2d, the addition of the satellite resonators leads to a change in the field distribution pattern and the formation of additional transmission peaks, indicating an increase in the number of resonance modes and an improvement in the filter's spectral performance.

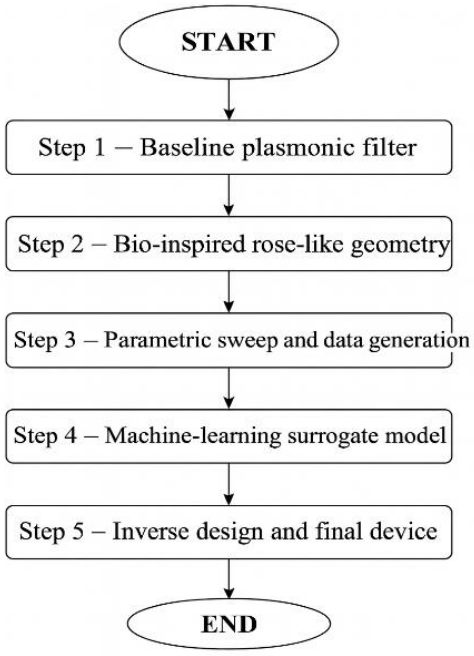

Fig. 3. The proposed flowchart of filter design.

The complete flowchart of the proposed design methodology is summarized in Fig. 3, which outlines the step-by-step progression from the baseline MIM filter to the bio-inspired rose geometry, the parametric sweep, and the surrogate-assisted inverse design.

B. Dual-Mode Operation and Physical Analysis Origin of the Performance

The observed dual-mode functionality of the rose-inspired filter is governed by the Fano resonance phenomenon. This effect arises from the interference between two distinct electromagnetic states: a spectrally broad 'bright mode' supported by the directly-coupled central resonator, and spectrally narrow 'dark modes' supported by the isolated satellite resonators [22, 26]. The bright mode facilitates a high-throughput pathway for light, corresponding to the high-transmission resonance. In contrast, the dark modes act as high-Q energy reservoirs, excited only indirectly via near-field coupling. The interference between these two pathways carves a sharp, asymmetric resonance out of the broad transmission spectrum, creating the high-selectivity, high Q-factor peak. This physical interpretation is definitely verified by our modal field investigation. It is evident from the latter that at the high-transmission resonance, energy is mainly concentrated within the central resonator and hence verifies its bright-mode nature. At the high-Q resonance, the field is highly localized within the satellite resonators and shows clear visual verification of the energy-storing dark modes. This scenario verifies that the structural geometry is absolutely designed such that it is capable of accommodating the Fano interference essential for its double-function functionality.

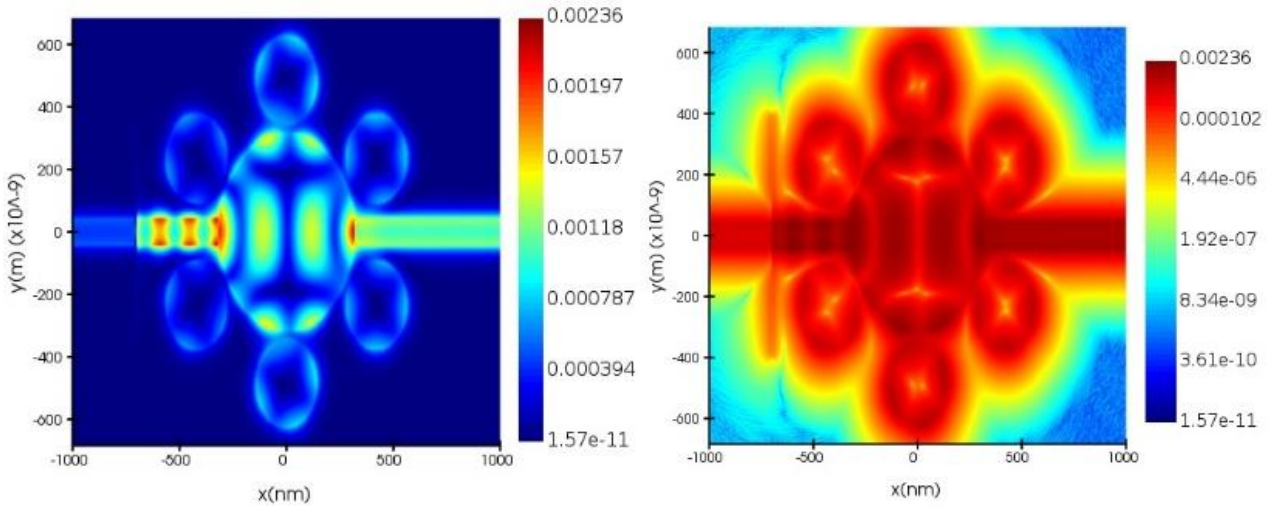

(a) (b)

Fig. 4. (a) Bright resonance at λ ≈ 774.2 nm, with the field being strongly coupled to the dominant waveguide and the central cavity. (b) Dark resonance at λ ~ 1145.5 nm, where the optical energy is mainly localized inside the satellite resonators with a sharp and high-Q resonance and small coupling to the waveguides. Such mode profiles demonstrate the plasmonic processes and thus meet the reviewer's demand for the visualization of field distributions for all resonance modes.

C. Parametric Optimization of the Rose-Inspired Structure

The rose-inspired geometry was defined, and then its dimensions were optimized through a thorough parametric analysis. Initially, the impact of the primary resonator radius (R) was examined. While keeping the small resonator radius constant at r = 140 nm, Fig. 5 contrasts the outcomes for three values of R: 300 nm, 310 nm, and 315 nm. It is evident that the main modes' transmission efficiency (T max) greatly increases as R rises. We specifically achieved the best performance in the R = 315 nm case, with a quality factor (Q-factor) of up to 127.2 and a transmission efficiency of up to 80% (see Table I for full details). Consequently, this arrangement was chosen as the main resonator's ideal radius.

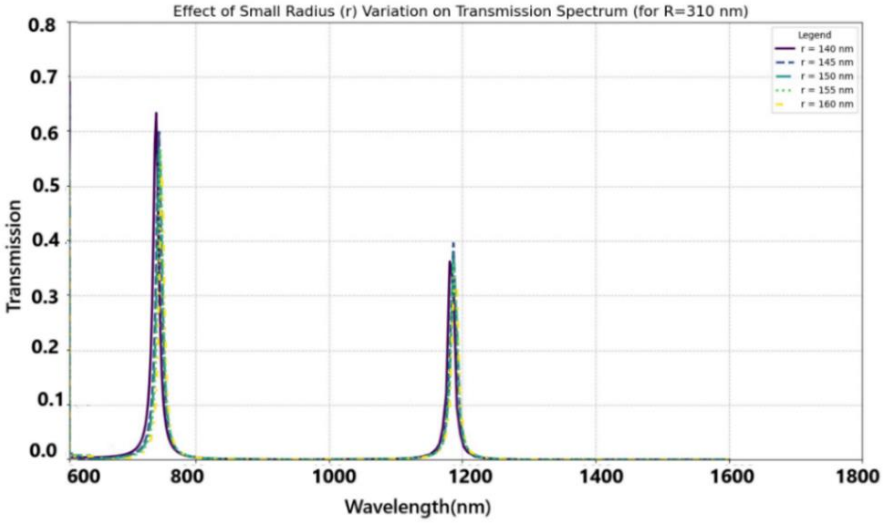

(a)

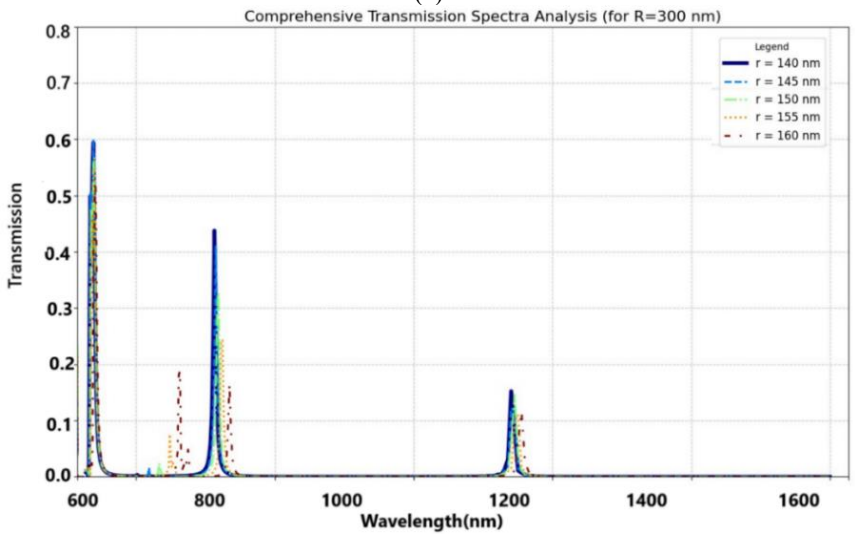

(b)

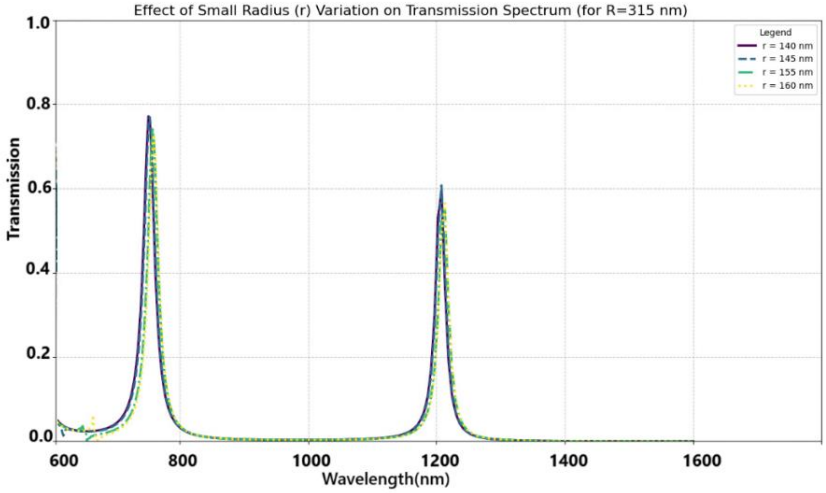

(c)

Fig. 5. Comparison of transmission spectra for three different main resonator radii (R), while keeping the satellite resonator radius constant (r=140 nm): (a) R = 300 nm, (b) R = 310 nm, and (c) R = 315 nm.

In the next step, to evaluate the fabrication tolerance and robustness of the optimized structure (R = 315 nm, r = 140 nm), the effect of variations in the gap (s) between the main waveguide and the resonator system was investigated. Fig. 6 shows that minor variations in this gap (from -10 to +10 nm) create predictable and gradual changes in the transmission spectrum, without disrupting the overall nature of the filter's performance. The plot shows that minor variations in the gap create predictable and gradual shifts in the resonance peaks, indicating the design's robustness against small fabrication processes.

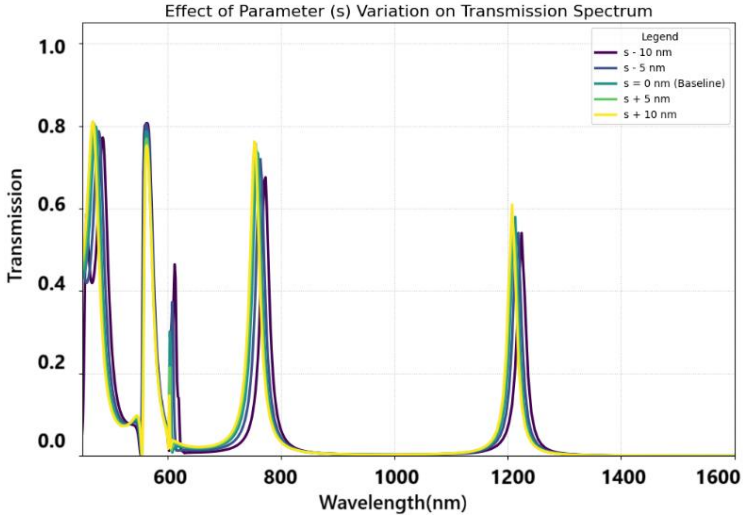

Fig. 6. Analysis of the effect of gap (s) variation on the transmission spectrum of the optimized structure (R = 315 nm, r = 140 nm).

D. The Machine Learning Surrogate Model's Performance

By contrasting the Random Forest model's predictions with FDTD simulation data that was not utilized during training, the model's accuracy was confirmed. As shown in Fig. 7 for the optimal structure (R=315nm), the simulated spectra (solid black line) and the AI-predicted spectra (red dashed line) match very well, achieving an R^2 score of 0.978.

For a more quantitative and detailed assessment of the model's performance, Fig. 8 presents a comparison of heatmaps. Fig. 8(a) shows the percentage prediction error across the parameter space. It is evident that the model performs extremely well in the overwhelming majority of parameter combinations, with a prediction error of less than 5% and reaching a minimum error of just 0.3% (for R=315 nm, r=150 nm). Fig. 8(b) visualizes the model's R^2 scores for the same parameter sweeps. These results quantitatively confirm the high accuracy and robustness of the model, with scores consistently above 0.93 and reaching a peak value of 0.986. This thorough analysis not only demonstrates the model's reliability for design and optimization but also precisely identifies the regimes of its highest performance.

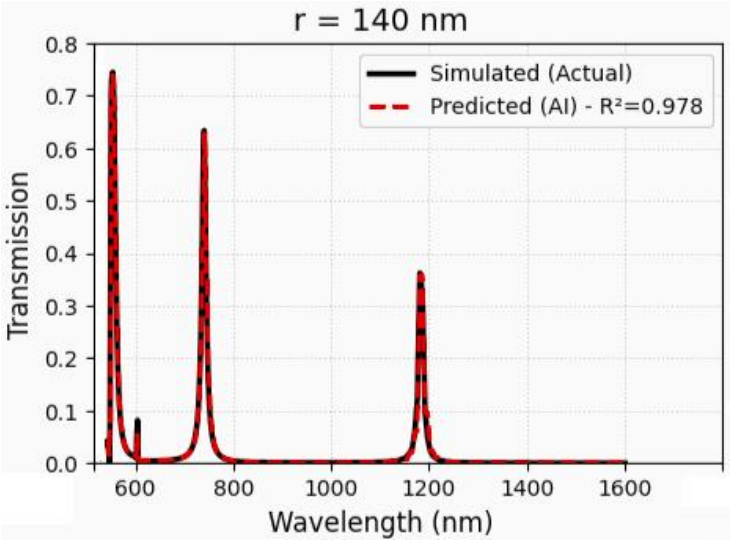

Fig. 7. Comparison of the FDTD-simulated (Actual) and the AI-predicted transmission spectra for the optimal filter configuration (R = 315 nm, r = 140 nm).

The high agreement between the two curves, confirmed by an R^2 score of 0.978, demonstrates the accuracy and reliability of the surrogate mode. Fig. 8 shows the percentage prediction error across the parameter space for a more quantitative and detailed assessment of the model's performance. The radius of the satellite resonator (r) is swept along the vertical axis of each map; however, the error heatmaps for three values of constant principal radii (R = 300, 310, and 315 nm) are compared here. Each cell in these maps shows the relative percentage error between

the FDTD-simulated spectrum and the AI-predicted spectrum. With a prediction error of less than 5%, the model performs extremely well in the overwhelming majority of parameter combinations, as evident from both the numerical values and the color scale (where lower error is indicated by darker color). The high accuracy and robustness of the model, as hinted earlier by the R^2 score, are quantitatively confirmed by these results. However, this thorough study also makes it clear that the error rate very slightly rises as the radius r becomes larger, especially in the case of R = 315 nm. In addition to demonstrating the reliability of the model for design and optimization, this transparency about the model's performance serves to precisely identify the regimes where the model falters.

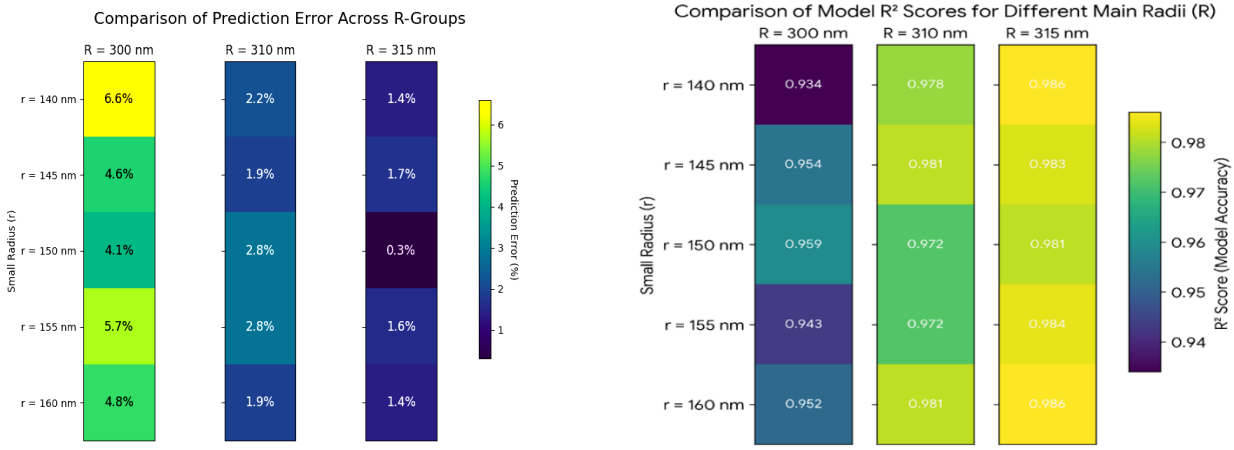

(a) (b)

Fig. 8: Heatmaps comparing the performance of the machine learning model across different geometries. (a) Prediction error percentage, where each column represents a constant main radius (R) and the vertical axis shows the variation of the satellite radius (r). Darker colors indicate lower error and higher agreement with FDTD simulations. (b) Model R^2 Scores for the same parameter sweeps. Brighter/warmer colors indicate higher model accuracy (a score closer to 1).

E. Performance Metrics and Comparison

To quantitatively evaluate the filter's performance, key metrics including the quality factor (Q-factor) and maximum transmission efficiency (T_{max}) were calculated. Table I summarizes these metrics for a set of configurations.

TABLE I
Calculated Performance Metrics for the Rose-Inspired Filter.

R (nm)	r (nm)	Mode	Resonance λ (nm)	Transmission (%)	FWHM (nm)	Q-factor
300	140	1	722.9	44.1	14.1	51.3
		2	1152.1	16.1	9.4	122.6
310	140	1	760.1	62.4	14.9	51.0
		2	1150.1	38.6	9.2	125.0
315	140	1	774.2	80.0	16.5	46.9
		2	1145.5	60.1	9.0	**127.2**

The primary advantage of our design lies in its dual-mode operation, wherein it fulfills two distinct functions within the same structure: a high-selectivity mode for sensing and a high-throughput mode for signal transmission. To numerically assess this unique trade-off, we introduce a Figure of Merit (FOM). The measure is designed to prefer structures that offer both a sharp, high-Q resonance (Mode 2) and another efficient high-transmission passband (Mode 1) simultaneously, encapsulating the practical usefulness in multi-functional integrated circuits. The FOM is expressed as:

$$\text{FOM} = \frac{Q_{mode2} \cdot T_{mode\,1}}{100}, \quad (2)$$

where QMode2 is the Fano sharp Mode 2 quality factor, and TMode1 is the percentage peak transmission of the broad bright-mode (Mode 1) resonance. Because of the requirement that a truly useful dual-mode device must excel in both areas, a multiplicative format was chosen. This FOM prevents the overall score from being seriously penalized if either the Q-factor or transmission is diminished and hence serves as a proper gauge of the device's real-world utility. In our thorough analysis, our proposed filter is tested against several state-of-the-art designs listed in Table II For easier comparison with single-mode filters, we have included the conventional Q × T Product figure of merit.

TABLE II
Comparison of the Proposed Plasmonic Filter with Reported Designs in the Literature

Reference (Year)	Resonator Structure	Resonance Wavelength (λ)	Q-factor	Transmission (T)	Q×T	FOM
This work (Mode 1)	Rose-Inspired Resonator	774.2 nm	46.9	80.0%	3752	101.76
This work (Mode 2)	Rose-Inspired Resonator	1145.5 nm	127.2	60.1%	7645	101.76
Korani et al. (2024) [28]	Ring with silver nanorods	1205.8 nm	207	93%	19251	N/A
Wang et al. (2022) [7]	Double split circular ring	591 nm	~49	~80%	~3920	N/A

Here is a comparison of our filter's performance metrics against other relevant works. As shown in Table II, our proposed filter exhibits competitive performance even in conventional figures of merit such as the Q × T product, especially in its high-Q mode. Although individual Q × T values may exceed those of specific single-mode designs or configurations, our structure is characterized by its double functionality. This distinguished feature is quantitatively reflected by our tailored FOM, which is found at a high level of 10176. This quantitatively points up our design's excellent multifunctional balance at the cost of conventional single-purpose filters.

V.CONCLUSION

In this research, we proposed a new, bio-inspired multichannel plasmonic filter based on a rose-shaped nanostructure and numerically characterized it. Sharp and controllable transmission peaks were attained, and the potential application for use in sophisticated filtering applications was demonstrated. To circumvent the computational expense of typical FDTD calculations, a tractable Random Forest-based surrogate model was formulated and calibrated. It is utilized to estimate the transmission spectra ($R^2 > 0.95$) very accurately, and the application of this model permits rapid design investigation and optimum design. The filter's proposed performance was compared against a number of state-of-the-art designs. Although other designs might provide slightly better transmission or peak Q-factors within a solitary mode, our design stands out due to its double-mode capabilities. Such superiority was numerically encapsulated in a specially-defined FOM, which provided a high number of about 102. This finding verifies the superior trade-off between two distinct operating regimes: a high-Q mode ($Q \approx 127.2$) suited for high-resolution sensing platforms and a high-transmission mode ($T \approx 80.0\%$), suited for applications where stable signal throughput is required. This tunability can be supported further by its comparable performance, rendering the rose-shaped filter a strong component for next-generation PICs, such as WDM systems and on-chip biosensors. Experimental confirmation of performance for the optimized design and exploration in its application in high-sensitivity sensing platforms will be addressed in later work. The dominant resonances at $\lambda \approx 774.2$ nm and $\lambda \approx 1145.5$ nm lie within the technologically important NIR region, making the filter highly suitable for compact wavelength-division multiplexing (WDM) modules and high-resolution refractive-index sensing applications. The coexistence of these modes enables simultaneous signal routing and sensing on the same photonic chip. Future work will focus on experimental validation of the proposed design and its integration into high-sensitivity plasmonic sensing platforms.

ACKNOWLEDGMENTS

This research was supported by Semnan University. Also, the authors would like to thank the editor and reviewers for their valuable comments.

FUNDING

No funding was received for this research.

CONFLICTS OF INTEREST

The third author is an Assistant Editor for Modeling and Simulation in Electrical and Electronics Engineering Journal and was not involved in the editorial review or the decision to publish this article.

DATA AVAILABILITY

All the data analyzed in this study are provided within this published article.

AUTHOR CONTRIBUTIONS

SMMH: Conceptualization, Methodology, Software, Validation, Writing – original draft, review & editing. PR: Methodology, Validation, Supervision, Writing – review and editing. SK: Methodology, Validation, Writing – review and editing.

REFERENCES

[1] S. Khani, P. Rezaei, and M. Rahmanimanesh, "Machine learning analysis of a Fano resonance-based plasmonic refractive index sensor using U-shaped resonators," *Scientific Reports*, vol. 15, p. 23857, 2025.

[2] S. Khani, M. Danaie, and P. Rezaei, "Design of a Single-Mode Plasmonic Bandpass Filter Using a Hexagonal Resonator Coupled to Graded-Stub Waveguides," *Plasmonics*, vol. 13, pp. 2177–2186, 2018.

[3] M. Aftab, M. S. Mansha, T. Iqbal, and M. Farooq, "Surface Plasmon Excitation: Theory, Configurations, and Applications," *Plasmonics*, vol. 19, pp. 1701–1719, 2024.

[4] S. A. Maier, "Plasmonics: Metal Nanostructures for Subwavelength Photonic Devices," *IEEE Journal of Selected Topics in Quantum Electronics*, vol. 12, no. 6, pp. 1214-1220, Nov. 2006.

[5] R. F. Oulton, G. Bartal, D. F. P. Pile, and X. Zhang, "Confinement and propagation characteristics of subwavelength plasmonic modes," *New Journal of Physics*, vol. 10, p. 105018, Oct. 2008.

[6] M. H. Fuad, M. F. Nayan, and R. R. Mahmud, "Advances in Surface Plasmon Resonance-Based PCF and MIM Sensors," *Plasmonics*, 2025.

[7] S Khani, M Hayati, Optical sensing in single-mode filters based on surface plasmon H-shaped cavities, Optics Communications, 2022, 505, 127534.rezaei

[8] M. Z. U. Rahman, T. C. E. Cheng, M. T. Islam, and N. Misran, "Ultra-Wide-Band Band-Pass Filters Using Plasmonic MIM Waveguide-Based Ring Resonators," *IEEE Photonics Technology Letters*, vol. 30, no. 19, pp. 1715-1718, Oct. 2018.

[9] S. Kumar, *et al*., "Nanophotonic Ring Resonator Based on Slotted Hybrid Plasmonic Waveguide for Biochemical Sensing," *IEEE Sensors Journal*, vol. 23, no. 6, pp. 5695-5702, Mar. 2023.

[10] F. Liu, Y. Cui, S. Yan, and B. Huang, "A MIM Waveguide Refractive-Index Construction According to SPPs and Fano Resonance," in *Proc. 5th Int. Conf. Intell. Control, Meas. Signal Process. (ICMSP)*, 2023, pp. 1011-1014.

[11] A. V. Maslov and M. Miyawaki, "Confinement factors and optical gain in subwavelength plasmonic resonators," *Journal of Applied Physics*, vol. 108, no. 8, p. 083105, Oct. 2010.

[12] S.A. Khatami, P. Rezaei, "Coupled mode theory analysis of the graphene-based multi-band superabsorber for selective sensing application," Diamond and Related Materials, vol. 158, 112690, 2025.

[13] A. L. Musgrove, *et al*., "Bio-inspired photonic and plasmonic systems for gas sensing: applications, fabrication, and analytical methods," *Journal of Optical Microsystems*, vol. 4, no. 2, p. 020902, 2024.

[14] Z. Jakšić, M. Obradov, and O. Jakšić, "Bio-Inspired Nanomembranes as Building Blocks for Nanophotonics, Plasmonics and Metamaterials," *Biomimetics*, vol. 7, no. 4, p. 222, Dec. 2022.

[15] A.H. Asl, M. Khajenoori, Green extraction in separation technology, CRC Press, 2021.

[16] S. Chugh, S. Ghosh, A. Gulistan, and B. M. A. Rahman, "Machine Learning Regression Approach to the Nanophotonic Waveguide Analyses," *Journal of Lightwave Technology*, vol. 37, no. 24, pp. 6080-6089, Dec. 2019.

[17] Z. Jakšić, S. Devi, O. Jakšić, and K. Guha, "A Comprehensive Review of Bio-Inspired Optimization Algorithms Including Applications in Microelectronics and Nanophotonics," *Biomimetics*, vol. 8, no. 3, p. 278, Jun. 2023.

[18] S.A. Khatami, P. Rezaei, P. Zamzam, S. Hadipour, S. Khani, "Smith chart analysis for transmission line method validation of a simple graphene-based absorber in sugar molecules detection," Results in Physics, vol. 77, pp. 108464, October 2025.

[19] P. Cheng, *et al*., "Bio-inspired self-assembly of large area 3D Ag@SiO2 plasmonic nanostructures with tunable broadband light harvesting," *Applied Materials Today*, vol. 25, p. 101238, 2021.

[20] M. K. Akbari, *et al*., "Bioinspired patterned photonic junctions for plasmon-enhanced metal photoluminescence and fluorescence: design of optical cavities for near-infrared electronics," *Materials Today Energy*, vol. 26, p. 101003, 2022.

[21] S. Khani, M. Danaie, P. Rezaei, "Tunable single-mode bandpass filter based on metal-insulator-metal plasmonic coupled U-shaped cavities," IET Optoelectronics, vol. 13, no. 4, pp. 161-171, 2019.

[22] H. Geng *et al*., "Symmetry Breaking Induced Multiple Fano Resonances for Plasmonic Nanosensing," *Plasmonics*, 2025, doi: 10.1007/s11468-024-02318-y.

[23] S. Javid, F. Tavakkol Hamedani, P. Rezaei, S. Khani, "Designing scalable single-mode to seven-mode plasmonic filters utilizing disk and ring-shaped resonators," Results in Optics, vol. 21, 100919, 2025.

[24] R. Jaswal, *et al*., "Plasmonic nanoparticle-integrated nanofibers: advancements in nanobiotechnology for biomedical applications," *Journal of Pharmaceutical Investigation*, 2025.

[25] J. Zhou, Z. Wu, C. Jin, and J. X. J. Zhang, "Machine learning assisted dual-functional nanophotonic sensor for organic pollutant detection and degradation in water," *npj Clean Water*, vol. 7, no. 1, p. 3, 2024.

[26] Y. Sharma, B. Joshi, and R. Zafar, "Split Ring Resonators-Based Plasmonics Sensor with Dual Fano Resonances," *IEEE Sensors Journal*, vol. 21, no. 5, pp. 6050-6056, Mar. 2021.

[27] A.R. Jalalvand, Z. Rashidi, M. Khajenoori, "Sensitive and selective simultaneous biosensing of nandrolone and testosterone as two anabolic steroids by a novel biosensor assisted by second-order calibration," Steroids, vol. 189, 109138, 2023.

[28] N. Korani, L. Hajshahvaladi, and M. Danaie, "Realization of a single-mode plasmonic bandpass filter based on a ring-shaped resonator and silver nanorods," *Optical and Quantum Electronics*, vol. 56, no. 23, 2024.

[29] Q. Wang, *et al*., "Research on fiber optic surface plasmon resonance biosensors: A review," *Photonic Sensors*, vol. 14, p. 240201, 2024.

[30] M. H. Ehsani, S. Alamdari, "Biomaterials: Fundamentals, processing, and applications. In: Ikhmayies, S.J. (eds) Advances in Biomaterials Research. Advances in Materials Research and Technology. Springer, 2025.

[31] S.M. Ebadi, S. Khani, Highly-miniaturized nano-plasmonic filters based on stepped impedance resonators with tunable cut-off wavelengths, Plasmonics 18 (4), 1607-1618, 2023.

[32] J. Wang, *et al*., "Bandpass Half-Mode Substrate Integrated Plasmonic Filters with Steep Roll-Offs," *IEEE Photonics Technology Letters*, vol. 37, no. 5, pp. 269-272, Mar. 2025.

[33] Palik, E. D. (Ed.), Handbook of Optical Constants of Solids, Vol. 1, Academic Press, New York, USA, 1985.